ATR-FTIR Spectroscopy Reveals Bond Formation During Bacterial Adhesion to Iron Oxide

Sanjai J. Parikh and Jon Chorover*

Department of Soil, Water and Environmental Science, The University of Arizona, 429 Shantz Building #38, Tucson, Arizona 85721

Received May 12, 2006. In Final Form: July 26, 2006

The contribution of various bacterial surface functional groups to adhesion at hematite and ZnSe surfaces was examined using attenuated total reflectance (ATR) Fourier transform infrared (FTIR) spectroscopy. When live *Shewanella oneidensis*, *Pseudomonas aeruginosa*, and *Bacillus subtilis* cells were introduced to a horizontal hematite (α-Fe_2O_3)-coated internal reflection element (IRE), FTIR peaks emerged corresponding to bacterial phosphate group binding. These IR peaks were not observed when bacteria were introduced to the uncoated ZnSe IRE. When cells were added to colloidal suspensions of α-Fe_2O_3 at pH 7, spectra included peaks corresponding to P−OFe and ν(COOH), the latter being attributed to bridging of carboxylate at mineral surface OH groups. Selected model organic compounds with P-containing functionalities (phenylphosphonic acid [PPA], adenosine 5′-monophosphate [AMP], 2′-deoxyadenyl-(3′→5′)-2′-deoxyadenosine [DADA], and deoxyribonucleic acid [DNA]) produce spectra with similar peaks corresponding to P−OFe when adsorbed to α-Fe_2O_3. The data indicate that both terminal phosphate/phosphonate and phosphodiester groups, either exuded from the cell or present as surface biomolecules, are involved in bacterial adhesion to Fe-oxides through formation of innersphere Fe-phosphate/phosphonate complexes.

1. Introduction

Contamination of soil and water from increased urbanization and industrialization threaten human and environmental health. Understanding the mechanisms controlling bacterial adhesion at mineral surfaces is critical for addressing environmental phenomena associated with the fate and transport of bacterial cells. These processes are central to both contamination and remediation of soil and groundwater supplies.[1−4] The chemical properties of bacteria and abiotic environmental surfaces influence their mutual adhesion in soils and aquatic systems. Long-range electrostatic forces can diminish adhesion when bacteria and substrate surfaces are of like charge.[5] In addition to electrostatic effects, short-range interactions are controlled by (1) chemical (covalent, ionic, hydrogen) bonding, (2) van der Waals forces, and (3) hydrophobic effects.[6] Microbial adhesion is also influenced by steric effects, which are particularly important for overlapping regions of polymer segments.[7] Steric effects can promote adhesion via bridging of surface macromolecules or inhibit it when biopolymer overlap is unfavorable.[8]

Bacteria and many environmental particles exhibit net negative surface charge at pH values typically encountered in natural aqueous systems.[9] For example, quartz and silica are negatively charged at pH > 2.0−3.0.[10] Adhesion of bacteria to negative-charged (e.g., silicate and natural organic) surfaces is thought to be mediated via interaction with cell-surface proteins[11] or hydrophobic interactions.[12] However, in weathering environments, many silicaceous surfaces become coated with a veneer of hydrous Fe oxide, which can confer net positive charge at circumneutral pH.[10] As a result, bacterial adhesion to Fe-oxides is often greater than that observed for silicates, with the difference being attributed to electrostatic attraction.[13−15]

Although favorable electrostatics likely contribute to bacterial adhesion at positively charged surfaces, direct bonding of cell surface macromolecules at mineral surface functional groups may also play a role.[11,16−24] The exterior surface of bacterial cells is comprised of extracellular polymeric substances (EPS), teichoic acids (Gram-positive bacteria), lipopolysaccharides (LPS; Gram-negative bacteria), and membrane-bound proteins that can potentially form coordinative bonds with functional groups at mineral surfaces. Biomolecule−surface complexes have been shown to be important to "conditioning film" formation by siderophores and/or EPS, and covalent bonding interactions appear to affect strong adhesion.[25,26] EPS is itself a heterogeneous mixture of polysaccharides, proteins, lipids, and nucleic acids.[18,27] The presence of nucleic acids in EPS and biofilms results from

* Corresonding author. E-mail: chorover@cals.arizona.edu.

(1) Matthess, G.; Pekdeger, A. *Sci. Total Environ.* **1981**, *21*, 149.
(2) Banning, N.; Toze, S.; Mee, B. J. *Microbiology (Reading, U.K.)* **2003**, *149*, 47.
(3) Abu-Ashour, J.; Lee, H. *Environ. Toxicol.* **2000**, *15*, 149.
(4) Corapcioglu, M. Y.; Haridas, A. *J. Hydrol.* **1984**, *72*, 149.
(5) Marshall, K. C.; Stout, R.; Mitchell, R. *J. Gen. Microbiol.* **1971**, *68*, 337.
(6) Marshall, K. C. *Adv. Colloid Interface Sci.* **1986**, *25*, 59.
(7) Neu, T.; Marshall, K. *J. Biomater. Appl.* **1990**, *5*, 107.
(8) Rijnaarts, H. H. M.; Norde, W.; Lyklema, J.; Zehnder, A. J. B. *Colloids Surf. B* **1999**, *14*, 179.
(9) Rijnaarts, H. H. M.; Norde, W.; Bouwer, E. J.; Lyklema, J.; Zehnder, A. J. B. *Colloids Surf. B: Biointerfaces* **1995**, *4*, 5.
(10) Sposito, G. *The Chemsitry of Soils*; Oxford University Press: New York, 1989.
(11) Gomez-Suarez, C.; Pasma, J.; Van Der Borden, A. J.; Wingender, J.; Flemming, H. C.; Busscher, H. J.; Van Der Mei, H. C. *Microbiology (Reading, U.K.)* **2002**, *148*, 1161.
(12) Salerno, M. B.; Logan, B. E.; Velegol, D. *Langmuir* **2004**, *20*, 10625.
(13) Truesdail, S. E.; Lukasik, J.; Farrah, S. R.; Shah, D. O.; Dickinson, R. B. *J. Colloid Interface Sci.* **1998**, *203*, 369.
(14) Bolster, C. H.; Mills, A. L.; Hornberger, G. M.; Herman, J. S. *J. Contam. Hydrol.* **2001**, *50*, 287.
(15) Deo, N.; Natarajan, K. A.; Somasundaran, P. *Int. J. Miner. Process.* **2001**, *62*, 27.
(16) Arredondo, R.; Garcia, A.; Jerez, C. A. *Appl. Environ. Microbiol.* **1994**, *60*, 2846.
(17) Makin, S. A.; Beveridge, T. J. *Microbiology (Reading, U.K.)* **1996**, *142*, 299.
(18) Wingender, J.; Neu, T. R.; Flemming, H. C. In *Microbial Extracellular Polymeric Substances: Characterization, Structure, and Function*; Wingender, J., Neu, T. R., Flemming, H. C., Eds.; Springer: Berlin, 1999; pp 1−15.
(19) Poortinga, A. T.; Bos, R.; Norde, W.; Henk, J. B. *Surface Sci. Rep.* **2002**, *289*, 1.32.
(20) Xu, L. C.; Logan, B. E. *Langmuir* **2006**, *22*, 4720.
(21) Xu, L. C.; Vadillo-Rodriguez, V.; Logan, B. E. *Langmuir* **2005**, *21*, 7491.
(22) Li, X.; Logan, B. E. *Langmuir* **2004**, *20*, 8817.
(23) Frank, B. P.; Belfort, G. *Langmuir* **1997**, *13*, 6234.
(24) de Kerchove, A. J.; Elimelech, M. *Langmuir* **2005**, *21*, 6462.

10.1021/la061359p CCC: $33.50
Published on Web 08/29/2006

extracellular production[28−31] and cell lysis.[32] Using Fourier transform infrared (FTIR) spectroscopy and quantum chemical calculations it was determined that EPS from *Pseudomonas aeruginosa* and *Bacillus subtilis* binds to Fe centers on goethite (α-FeOOH) via innersphere complexation of phosphate-bearing macromolecules.[25] A subsequent study showed that phosphate group binding also affects the partitioning of EPS macromolecules in aqueous goethite suspensions such that P-bearing macromolecules are adsorbed preferentially.[33] The formation of innersphere orthophosphate complexes at Fe oxide surfaces is well-known.[34−36] Together, these results suggest a potentially important role for phosphoryl groups in bacterial cell binding to oxide surfaces, but this has not been demonstrated unambiguously for live cells. If bacterial cell adhesion to Fe oxides does involve the formation of Fe−phosphoryl complexes, such bonding may help to explain the high affinity of cells for metal-oxide-coated surfaces.[13−15] It may also help to explain observations of extracellular nucleic acids during incipient biofilm formation,[31,37] the strong binding of these P-bearing molecules to soil particles,[38,39] and their preservation following cell death in freshwater,[40,41] brackish water,[41] and deep-ocean sedimentary[42] environments.

FTIR spectroscopy provides molecular-scale information on both organic and inorganic constituents involved in bacterial adhesion.[15,43,44] Attenuated total reflectance (ATR)-FTIR spectroscopy permits investigation of dipolar functional groups in close proximity (ca. ≤ 1 μm) to the interface between a sample and an internal reflection element (IRE) in the presence of water.[45] Since this penetration depth is comparable to the size of bacterial cells, information on surface interactions between cells and mineral substrates may be obtained by varying the physical-chemical properties of the cell-IRE interface. ATR-FTIR has been used previously for in situ interrogation of bacterial cells,[46−49] biofilms,[44−46,50] and extracted bacterial surface biomolecules[26,27,51,52] in aqueous systems.

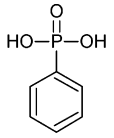

(a) Phenylphosphonic Acid (PPA)

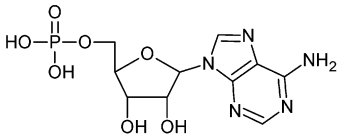

(b) Adenosine 5′-Monophosphate (AMP)

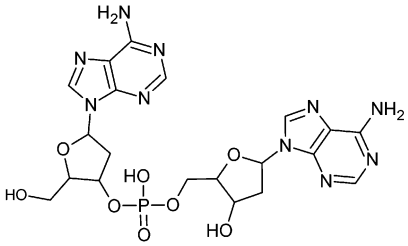

(c) 2'-Deoxyadenyl(3'→5')-2'-Deoxyadenosine (DADA)

Figure 1. Chemical structures of P-containing model compounds used for ATR-FTIR experiments.

In this study, we used ATR-FTIR to investigate the adhesion of live Gram-negative (*P. aeruginosa*, *Shewanella oneidensis*) and Gram-positive (*B. subtilis*) bacterial cells to a ZnSe IRE, and to the same IRE coated with nanohematite (α-Fe_2O_3) in oxic, aqueous systems. We also examined spectra obtained when the bacterial cells were subjected to heterocoagulation with the colloidal oxides in aqueous suspension. The primary objective was to elucidate the cell surface functional groups involved in bacterial adhesion to these different surfaces and to test the hypothesis that direct bonding to Fe metal centers is mediated by cell-surface phosphoryl groups. At circumneutral pH, the uncoated ZnSe IRE, with an isoelectric point (IEP) <4, serves as a model negative-charged surface,[53] while α-Fe_2O_3 (IEP = 8.0−8.5)[10] coatings provide a test of cell binding to a positive-charged Fe oxide surface at the same pH. We found that phosphate group binding was most apparent during cell adhesion to the α-Fe_2O_3-coated ZnSe. Band assignment and assessment of the role of phosphate/phosphonic groups in bacterial adhesion were facilitated by collection of ATR-FTIR spectra on selected model compounds.

2. Experimental Procedures

2.1. Bacteria and Growth Conditions. Bacteria were grown aerobically at 30 °C to the early stationary phase (10^5 cells mL^{-1}) in appropriate growth media as follows: *Shewanella oneidensis* (MR1) − tryptic soy broth,[54] 22 h; *Pseudomonas aeruginosa* (PAO1) and *Bacillus subtilis* (NRS 730) − Luria broth,[25,55] 24 h. Cells were harvested by centrifugation (3000*g*, 20 min, 4 °C) and washed once (100 mmol L^{-1} NaCl, pH 7) to remove growth media and free EPS. Live cells were then resuspended immediately in 100 mmol L^{-1} NaCl (pH 7) for FTIR experiments.

2.2. Chemicals and Solutions. All solutions were prepared in acid-washed glass vials using Barnstead Nanopure (BNP) water

(25) Omoike, A.; Chorover, J.; Kwon, K. D.; Kubicki, J. D. *Langmuir* **2004**, *20*, 11108.
(26) McWhirter, M. J.; Bremer, P. J.; Lamont, I. L.; McQuillan, A. J. *Langmuir* **2003**, *19*, 3575.
(27) Omoike, A.; Chorover, J. *Biomacromolecules* **2004**, *5*, 1219.
(28) Demain, A. L.; Burg, R. W.; Hendlin, D. *J. Bacteriol.* **1965**, *89*, 640.
(29) Muto, Y.; Goto, S. *Microbiol. Immunol.* **1986**, *30*, 621.
(30) Kadurugamuwa, J. L.; Beveridge, T. J. *J. Bacteriol.* **1995**, *177*, 3998.
(31) Whitchurch, C. B.; Tolker-Nielsen, T.; Ragas, P. C.; Mattick, J. S. *Science* **2002**, *295*, 1487.
(32) Sutherland, I. W. *Trends Microbiol.* **2001**, *9*, 222.
(33) Omoike, A.; Chorover, J. *Geochim. Cosmochim. Acta* **2006**, *70*, 827.
(34) Tejedor-Tejedor, M. I.; Anderson, M. A. *Langmuir* **1990**, *6*, 602.
(35) Persson, P.; Nilsson, N.; Sjoberg, S. *J. Colloid Interface Sci.* **1996**, *177*, 263.
(36) Arai, Y.; Sparks, D. L. *J. Colloid Interface Sci.* **2001**, *241*, 317.
(37) Steinberger, R. E.; Holden, P. A. *Appl. Environ. Microbiol.* **2005**, *71*, 5404.
(38) Cai, P.; Huang, Q. Y.; Zhang, X. W.; Chen, H. *Pedosphere* **2005**, *15*, 16.
(39) Ogram, A. V.; Mathot, M. L.; Harsh, J. B.; Boyle, J.; Pettigrew, C. A. *Appl. Environ. Microbiol.* **1994**, *60*, 393.
(40) Ogram, A.; Sayler, G. S.; Gustin, D.; Lewis, R. J. *Environ. Sci. Technol.* **1988**, *22*, 982.
(41) Ogram, A.; Sayler, G. S.; Barkay, T. *J. Microbiol. Methods* **1987**, *7*, 57.
(42) Dell'Anno, A.; Danovaro, R. *Science* **2005**, *309*, 2179.
(43) Benning, L. G.; Phoenix, V. R.; Yee, N.; Tobin, M. J. *Geochim. Cosmochim. Acta* **2004**, *68*, 729.
(44) Parikh, S. J.; Chorover, J. *Geomicrbiol. J.* **2005**, *22*, 207.
(45) Nivens, D. E.; Schmitt, J.; Sniatecki, J.; Anderson, T. R.; Chambers, J. Q.; White, D. C. *Appl. Spectrosc.* **1993**, *47*, 668.
(46) Nichols, P. D.; Henson, J. M.; Guckert, J. B.; Nivens, D. E.; White, D. C. *J. Microbiol. Methods* **1985**, *4*, 79.
(47) Naumann, D.; Helm, D.; Labischinski, H. *Nature* **1991**, *351*, 81.
(48) Sockalingum, G. D.; Bouhedja, W.; Pina, P.; Allouch, P.; Mandray, C.; Labia, R.; Millot, J. M.; Manfait, M. *Biochem. Biophys. Res. Commun.* **1997**, *232*, 240.
(49) Jiang, W.; Saxena, A.; Song, B.; Ward, B. B.; Beveridge, T. J.; Myneni, S. C. B. *Langmuir* **2004**, *20*, 11433.
(50) Schmitt, J.; Flemming, H. C. *Int. Biodeterior. Biodegrad.* **1998**, *41*, 1.
(51) Brandenburg, K. *Biophys. J.* **1993**, *64*, 1215.
(52) Parikh, S. J.; Chorover, J. In preparation **2006**.
(53) Tickanen, L. D.; Tejedor-Tejedor, M. I.; Anderson, M. A. *Langmuir* **1997**, *13*, 4829.
(54) Vinogradov, E.; Korenevsky, A.; Beveridge, T. J. *Carbohydr. Res.* **2003**, *338*, 1991.
(55) Nouwens, A. S.; Cordwell, S. J.; Larsen, M. R.; Molloy, M. P.; Gillings, M.; Willcox, M. D. P.; Walsh, B. J. *Electrophoresis* **2000**, *21*, 3797.

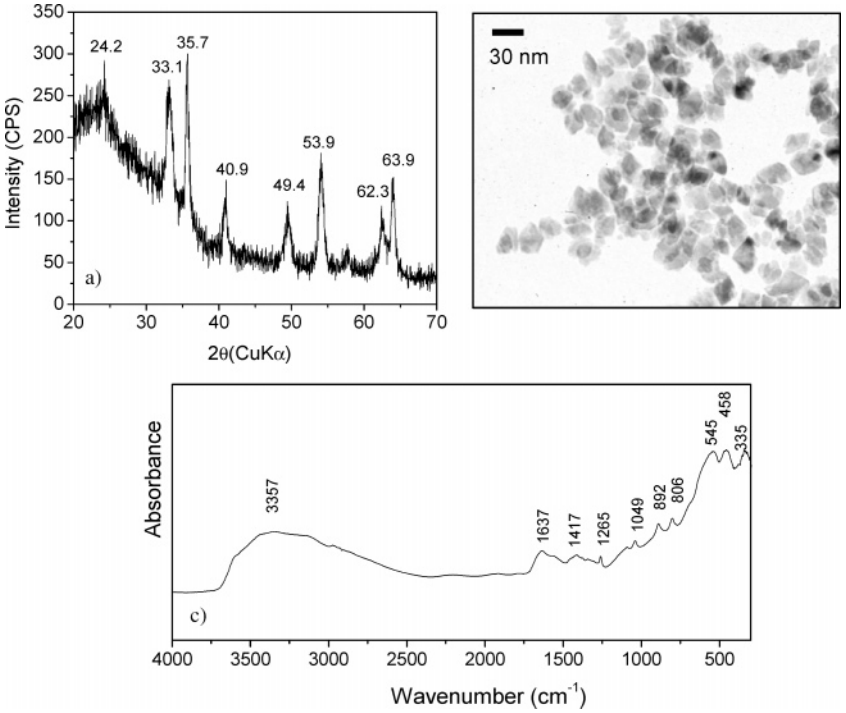

Figure 2. Characterization of synthetic α-Fe_2O_3 via (a) XRD, (b) TEM, and (c) DRIFT.

with pH adjustment via 100 mM NaOH/HCl. Solutions were prepared, stored overnight at 4 °C, and brought to room temperature before use. Phenylphosphonic acid (PPA; Sigma), adenosine 5′-monophosphate (AMP; Sigma), and the oligonucleotide, 2′-deoxyadenyl (3′→5′)-2′-deoxyadenosine (DADA; Operon) were each dissolved in 1.0 mM NaCl to give aqueous concentrations of 8, 4, and 3.5 mg mL^{-1}, respectively, at pH 7. Chemical structures for these compounds are given in Figure 1. Deoxyribonucleic acid (DNA; MP Biomedicals) from *Escherichia coli* was dissolved in 1.0 mM NaCl to give a final DNA concentration of 5 mg mL^{-1}.

2.3. Hematite Preparation and Analysis. Colloidal hematite (α-Fe_2O_3) particles were synthesized using the method of Schwertmann and Cornell.[56] Briefly, 100 mL of 1.0 M $Fe(NO_3)_3$ were added dropwise to 1 L of boiling BNP water over a 4 h period. The solution was allowed to cool overnight at room temperature. Removal of NO_3^- from the suspension required four repeated washing/flocculation steps in 100 mM NaCl. The α-Fe_2O_3 was resuspended in BNP water adjusted to pH 4 and dialyzed against the same with exterior solution changed twice daily (Spectra/Por 7 1000 MWCO, Spectrum).[57] Dialysis was considered complete when pH and electrical conductivity (EC) were unchanged over a 12 h period (pH 4, EC ∼ 110 μS cm^{-1}). The suspension concentration of α-Fe_2O_3 was determined by freeze-drying an aliquot of the colloidal suspension and measuring the residual mass.

Mineral composition and purity for α-Fe_2O_3 was confirmed by X-ray diffraction (XRD) using a Scintag XDS 2000 with a Cu X-ray source (40 kV and 40 mA), scan speed of 2° 2θ min^{-1}, and a step width of 0.03° 2θ. The particle size of synthetic α-Fe_2O_3 was determined by transmission electron microscopy (TEM) of particles mounted on 200 mesh copper grids after placing carbon coated mica into a drop of suspension and floating carbon/α-Fe_2O_3 onto the grid. Samples were observed at 60 kV with a JEOL JEM-100CX II electron microscope. Diffuse reflectance FTIR (DRIFT) spectra were also collected for α-Fe_2O_3 characterization. Freeze-dried α-Fe_2O_3 was diluted with KBr to approximately 10% (w/w) by gently mixing 39 mg of sample with 30 mg of KBr for 40 s and then folding in an additional 390 mg of KBr to homogenize the samples. DRIFT spectra were collected using a Nicolet 560 Magna IR spectrometer (Madison, WI) with 400 scans at 4 cm^{-1} resolution.

2.4. ATR-FTIR Spectroscopy and Analysis. ATR-FTIR spectra were collected using a 45° ZnSE IRE (Spectra-Tech ARK ATR cell) at pH 7, with 100 or 1.0 mM NaCl as background electrolyte. Spectra were acquired for each bacterial strain added as a cell suspension by three methods: (i) deposited directly onto the IRE surface, (ii) mixed with colloidal α-Fe_2O_3 and then deposited onto the IRE surface, and (iii) deposited onto a colloidal α-Fe_2O_3-coated IRE surface (i.e., colloidal films). Spectra for DNA, DADA, AMP, and PPA solution samples were collected using the ZnSe IRE with and without a α-Fe_2O_3 coating.

For sample introduction mode (ii), where cell-oxide contact was made prior to introduction into the ATR compartment, samples were prepared by adding cells to a suspension of colloidal α-Fe_2O_3 to give a final suspension comprising 1.96 g L^{-1} oxide and 5 × 10^5 cells mL^{-1} at pH 7.1. The suspension was immediately deposited on the IRE via pipet for data acquisition. For sample introduction mode (iii), metal oxide IRE coatings were prepared by drying the appropriate suspension (6 mL of α-Fe_2O_3 at 1.96 g L^{-1}) on the ZnSe IRE under vacuum (10 mmHg) overnight. After drying, films were gently rinsed with BNP water to remove loosely adhered material. New α-Fe_2O_3 coatings were prepared for each experiment, and spectra of dry oxide films were acquired each time to determine consistency of coatings and to permit calculation of difference spectra. Spectra were collected at 0, 15, 30, 45, 60, 90, 120, 150, 180, 210, and 240 min after sample introduction. All FTIR spectra were collected with 400 scans at a 4 cm^{-1} resolution using the corresponding electrolyte solution as background. For acquisition of sample spectra, the appropriate background spectrum (i.e., background electrolyte on ZnSe, α-Fe_2O_3 IRE coatings in background electrolyte, or colloidal α-Fe_2O_3 suspensions in background electroyte) was used to eliminate IR peaks arising from metal oxide vibrations. Collection of spectra was repeated with duplicate samples to ensure reproducible results. Time-dependent changes in spectral data were assessed by comparing relative changes in peak intensities of IR-absorbing functional groups. Confirmation of final pH (pH 7.0 ± 0.4) was conducted at the termination of the experiment. Peak fitting for quantitative comparisons was performed using GRAMS/AI (Thermo Electron Co.) software. The areas of Gaussian fitted peaks were used to determine relative spectral contributions of specific biomolecular components. DNA removal from the ATR crystal employed a cleaning solution

(56) Schwertmann, U.; Cornell, R. M. *Iron oxides in the Laboratory: Preparation and Characterization*; Wiley-VCH: Weinheim, Germany, 1991.
(57) Liger, E.; Charlet, L.; Van Cappellen, P. *Geochim. Cosmochim. Acta* **1999**, *63*, 2939.

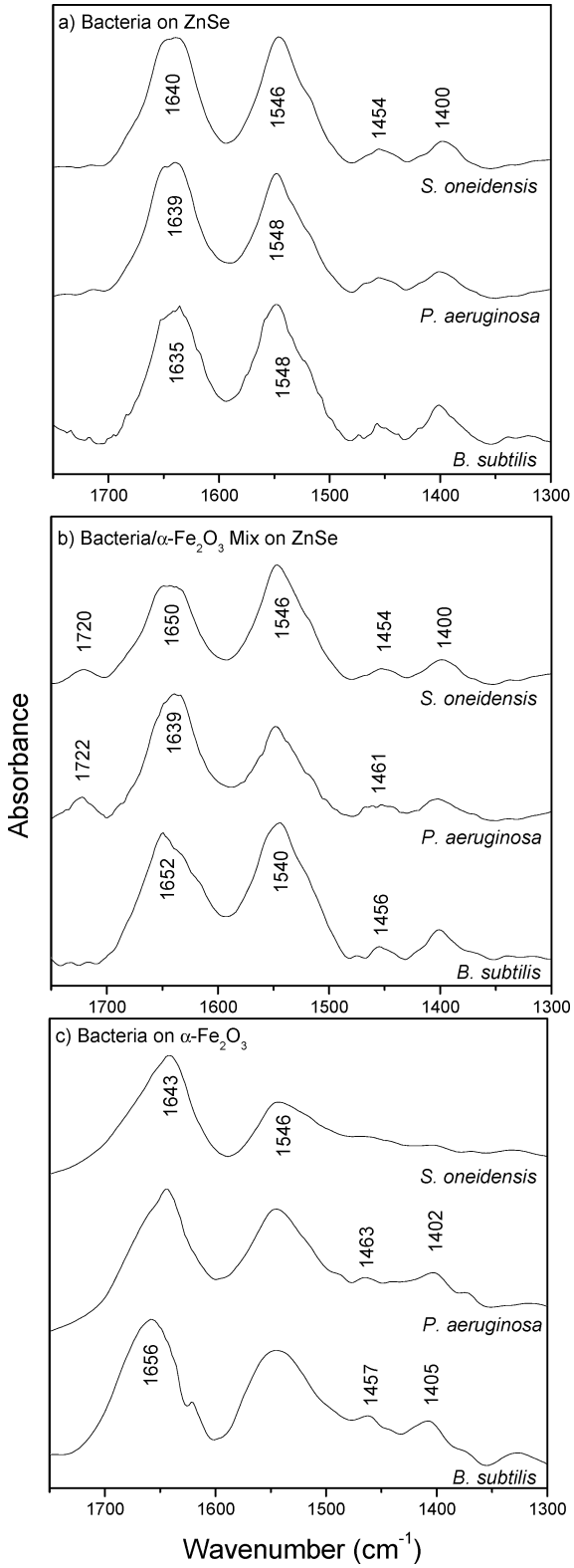

Figure 3. ATR−FTIR spectra (1750−1300 cm^{-1}) of *S. oneidensis*, *P. aeruginosa*, and *B. subtilis* (a) on ZnSe, (b) following aggregation with α-Fe_2O_3, and (c) on α-Fe_2O_3 film (all spectra collected after 240 min). Contact with α-Fe_2O_3 leads to decreased amide I and amide II contributions to the spectra accompanied by protein conformation/composition change.

of 10 mM Tris HCl (pH 8), 5 mM NaCl, and 1 mM EDTA at approximately 40 °C.[58]

(58) Stepanyugin, A. V.; Samijlenko, S. P.; Martynenko, O. I.; Hovorun, D. M. *Spectrochim. Acta, Part A* **2005**, *61*, 2267.

Table 1. IR Assignments for Bacteria and Biomolecules

wavenumber (cm^{-1})	IR band assignment
1720−1729	υ_{as}(COOH)[a,27,49,62]
1652−1637	amide I: C═O, C−N, N−H[45,48−50]
1550−1540	amide II: N−H, C−N[48−50,62]
1454−1482	$\delta(CH_2)$[b,45,62,63]
1360−1450	$\upsilon_s(COO^-)$[c,48,49,62,63]
1220−1260	$\upsilon_{as}(PO_2^-)$[62,64,65]
1170	υ(C−O)[45]
1137	$\upsilon_s(PO_2^-)$[25 66]
1114−1118	υ(C−O−P, P−O−P), ring vibrations[45,62]
1106−1108	$\upsilon_{as}(PO_3^{2-})$[67]
1084−1094	$\upsilon_s(PO_2^-)$,[25,64,65,68] ring vibrations,[62] υ(C−O)[65]
1078	υ_s(C−O−C, C−C),[68] $\upsilon(PO_3^{2-})$[48]
1048−1060	υ(C−O−C, C−C)[62,65]
1042−1046	$\upsilon_s(PO_3^{2-})$[67]
1039−1043	υ(P−OH, P−OFe)[25,69,70]
1016−1020	υ(P−OFe),[70] ring vibrations[62]
979	$\upsilon(PO_3^{2-})$[70]
974	υ(P−OH)[70]
962−970	$\nu(PO_2^-)$[63,70]

[a] ν_{as} = asymmetric stretching vibration. [b] δ = bending vibrations. [c] ν_s = symmetric stretching vibration.

3. Results

3.1. Metal Oxide Characterization. Synthesis of α-Fe_2O_3 was confirmed via XRD, TEM, and DRIFT analysis (Figure 2). Diffraction patterns show broad XRD peaks (consistent with small particle size) with *d* spacings consistent with hematite.[59] TEM micrographs reveal unidimensional crystals of rhomboid to hexagonal geometry measuring 10−20 nm across. The α-Fe_2O_3 DRIFT spectra display prominent peaks at 454 and 458 cm^{-1} corresponding to the Fe−O vibrations of hematite.[60] The spectra include distinct Fe−OH stretching (894 cm^{-1}) and bending (806 cm^{-1}) vibrations resulting from the high specific surface area and, hence, high surface hydroxyl group density of the nanoscale precipitates.[56,61] A broad peak at 3340 cm^{-1} corresponds to OH stretching frequencies that may include some contribution from adsorbed water.[61]

3.2. ATR-FTIR Spectra of Bacteria. Figure 3 shows the region from 1750 to 1300 cm^{-1} (comprising protein and carboxyl) for the three bacterial strains and three different treatments. The most prevalent features in these spectra correspond to amide I and amide II vibrations of proteins at ca. 1640 and 1550 cm^{-1}, respectively (Table 1). For the Gram-negative strains, *P. aeruginosa* and *S. oneidensis*, a smaller peak at ∼1720 cm^{-1}, corresponding to protonated carboxyl groups (also see section 4.2), is present consistently for cells aggregated with colloidal α-Fe_2O_3 (Figure 3b). This peak is not observed for Gram-positive *B. subtilis*. The COOH peak is also not observed when *P. aeruginosa* and *S. oneidensis* are introduced to the α-Fe_2O_3-coated IRE, irrespective of ionic strength (identical spectra were obtained in 1 and 100 mM NaCl), nor in any of the other treatments. Although the symmetric carboxylate stretch contributes to the band at ca. 1450 cm^{-1}, the asymmetric COO− stretch is masked by the strong amide II vibration, as has been shown in prior ATR-FTIR studies using D_2O as solvent.[27]

In the presence of α-Fe_2O_3, particularly when cells were introduced to the α-Fe_2O_3-coated IRE (Figure 3c), a decrease in

(59) Blake, R. L.; Hessevick, R. E.; Zoltai, T.; Finger, L. W. *Am. Mineral.* **1966**, *51*, 123.

(60) Schwertmann, U.; Taylor, R. M. In *Methods of Soil Analysis, Part 1− Physical and Mineralogical Methods*; Klute, A., Ed.; SSSA: Madison, WI, 1989; Vol. 5, pp 379−438.

(61) Farmer, V. C. *The infrared spectra of minerals*; Mineralogical Society: London, 1974.

peak intensity at ~1400 (COO^-) and ~1454 cm^{-1} (CH_2) is observed relative to the case with ZnSe IRE only (Figure 3a) (most apparent for *S. oneidensis*). For all three bacteria, there is a decrease in intensity of the amide II (~1550 cm^{-1}) relative to amide I (~1640 cm^{-1}) upon adhesion to the α-Fe_2O_3-coated IRE. Contact with α-Fe_2O_3, either via aggregation or colloidal film, results in an increase in frequency of the amide I peak for all three strains. No shift in the amide II region is observed.

The ATR spectral region comprising polysaccharide and phosphate (1300−950 cm^{-1}) is shown in Figure 4. Spectra for cells on ZnSe alone (Figure 4a) are similar across bacterial strains with the exception of the broad shoulder at 1045 cm^{-1} (C−O, C−O−C) for *B. subtilis*. Only a slight change in the spectra of Gram-negative bacteria (*P. aeruginosa*, *S. oneidensis*) is observed when cells are aggregated with colloidal α-Fe_2O_3 prior to emplacement on the ZnSe IRE (Figure 4b; α-Fe_2O_3 subtracted). In this case, a small peak at 1018 cm^{-1} (P−OFe) is observed and the broad peak from 1200 to 1260 cm^{-1} (PO_2^-) is better defined. When *B. subtilis* cells are mixed with α-Fe_2O_3, a sharp and intense peak (P−OFe) emerges at 1016 cm^{-1}, and the peak at ~1041 cm^{-1} (P−OFe) is increased relative to 1085 cm^{-1} (ring vibrations or PO_2^- [ν(ring-PO_2^-)]).

Spectra of cells introduced to α-Fe_2O_3 colloidal films are similar for all three bacteria (Figure 4c) but quite different from data collected under other conditions. These spectra are characterized by a reduction in peak intensity for the phosphate region between 1200 and 1260 cm^{-1} (particularly for Gram-negative cells), and they are dominated by C−C, C−O−C ring vibrations, PO_2^- (1087 cm^{-1}), and P−OFe complexes (1041 cm^{-1}). Consistency in spectra for bacterial interactions under the various conditions indicates a high degree of experimental reproducibility. In all cases where striking differences are observed in spectra (e.g., Figure 4b, *B. subtilis* aggregated with α-Fe_2O_3), additional replicate experiments were conducted to verify results.

3.3. Spectral Analysis. Peak fitting was performed on spectra presented in Figures 3 and 4 to determine the relative contributions of specific functional groups under the experimental conditions. Chi-squared values for peak fitting ranged from 0.0004 to 0.2483 and R^2 values were consistently 0.99−1.00. Peak area ratios were determined using Gaussian fits to major IR vibrational modes (Table 2). Comparing across data for cells on the ZnSe IRE, values for *B. subtilis* indicate a higher contribution of sugar rings to the spectra. The amide I:amide II ratio is 1.0 for ZnSe. However, this ratio is increased upon cell adhesion to the α-Fe_2O_3 IRE coating (1.27−3.45). For all bacteria, the ν(ring-PO_2^-): amide II ratio increases upon bacterial interaction with α-Fe_2O_3 colloidal film. Large decreases in the ν_{as}(PO_2^-):amide II and ν(ring-PO_2^-):amide II are observed for *B. subtilis* aggregated with colloidal α-Fe_2O_3, whereas changes for the Gram-negative bacteria are much smaller. For cells aggregated with colloidal α-Fe_2O_3, the contribution of Fe-phosphate complexes (~1016 cm^{-1}) is greatest for *B. subtilis*.

Kinetic data were collected to observe time-dependent spectral changes associated with bacterial adhesion under the three conditions studied (spectra not shown). Analysis of these data makes use of time dependent changes in peak intensities normalized to amide II. Only minor time-dependent changes were observed for bacterial cells aggregated with colloidal α-Fe_2O_3 or placed on the ZnSe IRE (not shown). However, when cells were introduced to the α-Fe_2O_3 colloidal film, these band intensity ratios were observed to increase in several cases indicating increased relative contributions of polysaccharide and phosphate groups at the solid−liquid interface (Figure 5). Time-dependent changes in ν(ring-PO_2^-):amide II and ν(P−OFe):

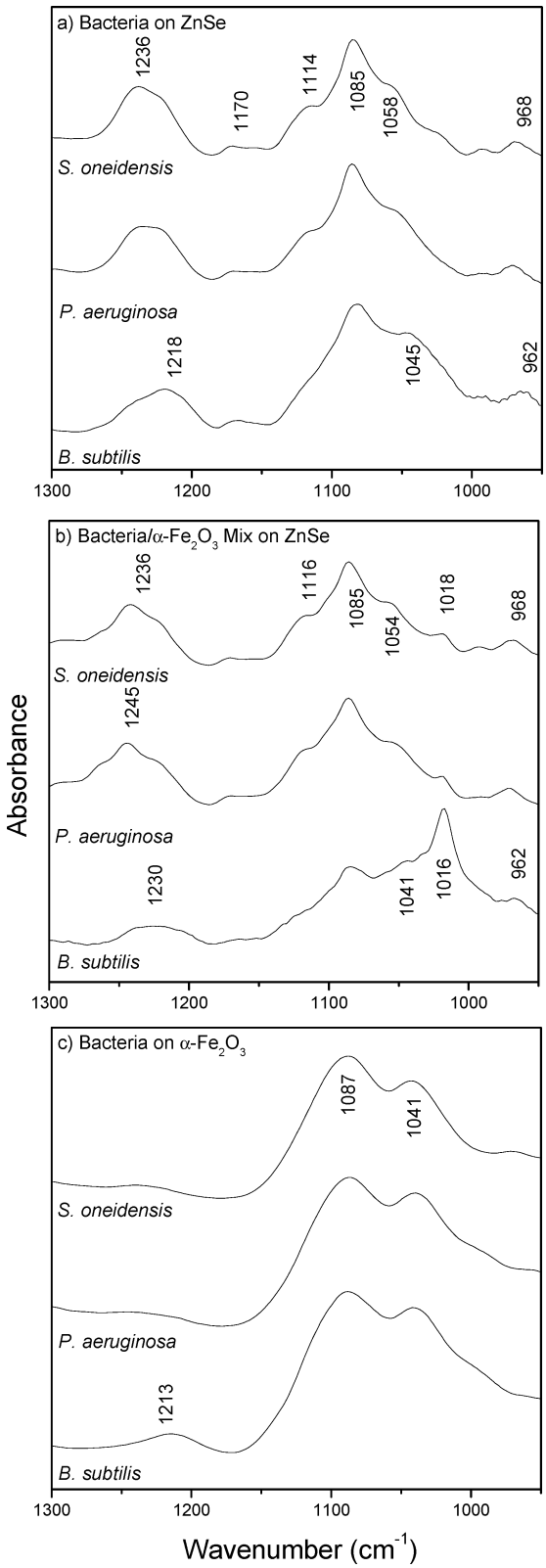

Figure 4. ATR−FTIR spectra (1300−950 cm^{-1}) of *S. oneidensis*, *P. aeruginosa*, and *B. subtilis* (a) on ZnSe, (b) following aggregation with α-Fe_2O_3, and (c) on α-Fe_2O_3 film (all spectra collected after 240 min). Contact with α-Fe_2O_3 results in growth of 1087 cm^{-1} peak (ring vibrations/phosphate) and inner-sphere P−OFe complexation as observed in the 1041 cm^{-1} peak.

amide II (1041 cm^{-1}) for bacteria on α-Fe_2O_3 films are correlated. Linear regression analysis of absorbance intensity at 1087 versus 1041 cm^{-1} give low p values (<0.0001 for all bacteria) and high correlation coefficients for bacteria on α-Fe_2O_3 films (*S. oneidenis*,

Table 2. ATR−FTIR Peak Area Ratios for Major Bacterial Functional Groups after 240 min Following (i) Addition to ZnSe, (ii) Aggregated with Colloidal α-Fe_2O_3 and Added to ZnSe, and (iii) Added to α-Fe_2O_3-Coated ZnSe

ATR-FTIR sample	amide I: amide II:	phosphate:[a] amide II	ring vibrations:[b] amide II	Fe−phosphate:[c] amide II	COOH: amide II
Bacteria on ZnSe					
S. oneidensis	1.06	0.22	0.17		
P. aeruginosa	1.04	0.25	0.25		
B. subtilis	0.97	0.10	0.75		
Bacteria/α-Fe_2O_3 on ZnSe					
S. oneidensis	0.92	0.19	0.21	0.04	0.06
P. aeruginosa	1.06	0.26	0.25	0.02	0.07
B. subtilis	0.98	0.06	0.21	0.11	
Bacteria on α-Fe_2O_3					
S. oneidensis	3.45	0.31	5.26	1.72	
P. aeruginosa	1.45	0.12	1.75	0.62	
B. subtilis	1.27	0.19	2.71	1.37	

[a] Phosphate peak areas correspond only to peaks present between 1200 and 1260 cm^{-1}. [b] Ring vibrations and/or PO_2^-; υ(ring-PO_2^-). [c] Fe−phosphate peak is 1016−1018 cm^{-1} for bacteria/α-Fe_2O_3 mix on ZnSe and 1041 cm^{-1} for bacteria on α-Fe_2O_3-coated ZnSe.

$R^2 = 0.9949$; *P. aeruginosa*, $R^2 = 0.9996$; *B. subtilis*, $R^2 = 0.9904$), suggesting that phosphate groups forming Fe complexes are associated with sugar ring structures.

3.4. ATR Spectra of DNA and Model P-Containing Molecules. ATR spectra (1300−950 cm^{-1}) collected after contacting DNA, DADA, AMP, and PPA solutions with ZnSe and α-Fe_2O_3 surfaces are shown in Figure 6. Sorbate spectra (following subtraction of the solid phase) show dependence on the chemical composition of the solution−IRE interface. Spectra for α-Fe_2O_3 (compared to ZnSe) indicate shifts in peak location and/or emergence of new peaks for each of the compounds studied.

Following contact with α-Fe_2O_3, the spectrum of DNA shows small peaks at 1022 (C−O, C−C), 998, and 1145 cm^{-1} [ν(P−OFe)].[25,69] Whereas DNA on ZnSe is characterized by strong amide I peaks (1641 and 1650 cm^{-1}, respectively), interaction with α-Fe_2O_3 films results in a much larger peak at 1577 cm^{-1} (amide II) and a new peak at 1400 cm^{-1}, consistent with υ_s(COO^-) (Figure 7).

The spectrum of the oligonucleotide, DADA, on the α-Fe_2O_3 film contains a strong vibration at 989 cm^{-1} [ν(P−OFe)][69,70] which is absent for other surfaces (Figure 6b). There is also loss of the peak at 1093 cm^{-1} (ring vibrations/PO_2^-) for DADA on the α-Fe_2O_3 film. Spectra for AMP on all three surfaces (Figure 6c) are similar to those observed for DADA. AMP on ZnSe shows a strong peak at 977 cm^{-1} [ν(PO_3^{2-})/P−OH]. AMP reacted with α-Fe_2O_3 produces an apparent peak shift from 977 (on ZnSe) to 993 cm^{-1} ([ν(P−OFe)]. This is accompanied by a shift of the 1083 cm^{-1} peak to 1074 cm^{-1}, both of which correspond to ring vibrations and/or PO_2^-.

Reaction of PPA with α-Fe_2O_3 leads to significant spectral changes, as compared to ZnSe (Figure 6d). New peaks are observed at 1091 (ring vibrations/PO_2^-), 1049 (C−O−C, C−C), and 1045 cm^{-1} (PO_3^{2-} or P−OFe). There is a large increase in intensity of the peak at ∼1137 cm^{-1} (PO_2^-) and a shift in the 968 cm^{-1} peak to 975 cm^{-1} is observed, indicating binding of the phosphonic group to Fe.

4. Discussion

4.1. Interpretation of Spectral Changes of Bacterial Amide Groups. IR peak areas normalized to that of amide II are used to determine protein conformational changes and/or changes in composition or bonding of biomolecules at the solid−liquid interface (Table 2). The amide I:amide II ratio can be used to differentiate changes in protein secondary structure.[71] For example, a conformational change in surface proteins is evident when bacteria bind to the α-Fe_2O_3-coated IRE. For bacteria on ZnSe (including cells aggregated with colloidal α-Fe_2O_3), the ratio is close to unity (0.92−1.06), whereas adhesion to α-Fe_2O_3 films induces a significant increase in this ratio (1.27−3.45). Also, the observed amide I peak shifts to higher wavenumber when cells, particularly those of Gram-positive *B. subtilis*, come into contact with α-Fe_2O_3 surfaces (Figure 3). These band shifts (e.g., 1635 cm^{-1} [ZnSe] to 1652 cm^{-1} [α-Fe_2O_3 mix] and 1656 cm^{-1} [α-Fe_2O_3 film]), may represent a change in protein conformation from β-sheet to α-helix structure.[72,73] The shift for the Gram-negative bacteria is smaller (*S. oneidensis:* 1640 cm^{-1} to 1650 cm^{-1} [α-Fe_2O_3 mix] and 1643 cm^{-1} [α-Fe_2O_3 film]; *P. aeruginosa:* 1639 cm^{-1} to 1639 cm^{-1} [α-Fe_2O_3 mix] and 1643 cm^{-1} [α-Fe_2O_3 film]) and may signal a change from β-sheet to random coil structures.[73] EPS extracted from *B. subtilis* and *P. aeruginosa* exhibited very similar shifts in the amide I peak, from 1643 to 1652 cm^{-1} and 1648 to 1657 cm^{-1}, respectively, after adhesion to goethite.[25] From analysis of amide I:amide II area ratios and peak shifts of the amide I, it is apparent that when bacteria interact with the α-Fe_2O_3 surface the proteins involved are of different composition and/or altered conformation relative to the case for interaction with the ZnSe surface.

Along with changes in protein conformation/composition there is also a decrease in overall protein absorbance (relative to polysaccharide and phosphate) upon adhesion to α-Fe_2O_3-coated IRE as compared to adhesion to the ZnSe IRE (Table 2). This suggests that cell adhesion to Fe oxide is not dominated by cell surface proteins, whereas these constituents play a more prominent role in deposition on ZnSe. The isoelectric point for ZnSe is pH

(62) Brandenburg, K.; Seydel, U. In *Infrared Spectroscopy of Biomolecules*; Mantsch, H. H., Chapman, D., Eds.; John Wiley and Sons: New York, 1996; pp 203−237.
(63) Quiles, F.; Burneau, A.; Keiding, K. In *Effect of Mineral-Organic Microorganism Interactions on Soil and Freshwater Environments*; Berthelin, J., Huang, P. M., Bollag, J.-M., Andreuz, F., Eds.; Klumer Academic/Plenum Publishers: New York, 1999; pp 133−142.
(64) Naumann, D.; Schultz, C. P.; Helm, D. In *Infrared Spectroscopy of Biomolecules*; Mantch, H. H., Chapman, D., Eds.; John Wiley and Sons: New York, 1996; pp 279−310.
(65) Fringeli, U. P.; Günthard, H. H. In *Membrane Spectroscopy*; Grell, E., Ed.; Springer-Verlag: Berlin, 1981; pp 270−332.
(66) Joshi, V. S.; Joshi, M. J. *Cryst. Res. Technol.* **2003**, *38*, 817.
(67) Socrates, G. *Infrared and Raman characteristic group frequencies: tables and charts*; Wiley: New York, 2001.
(68) Cepus, V.; Scheidig, A. J.; Goody, R. S.; Gerwert, K. *Biochemistry* **1998**, *37*, 10263.
(69) Sheals, J.; Sjoberg, S.; Persson, P. *Environ. Sci. Technol.* **2002**, *36*, 3090.
(70) Barja, B. C.; Tejedor-Tejedor, M. I.; Anderson, M. A. *Langmuir* **1999**, *15*, 2316.
(71) Ishida, K. P.; Griffiths, P. R. *Appl. Spectrosc.* **1993**, *47*, 584.
(72) Byler, D. M.; Susi, H. *Biopolymers* **1986**, *25*, 469.
(73) Buijs, J.; Norde, W.; Lichtenbelt, J. W. T. *Langmuir* **1996**, *12*, 1605.

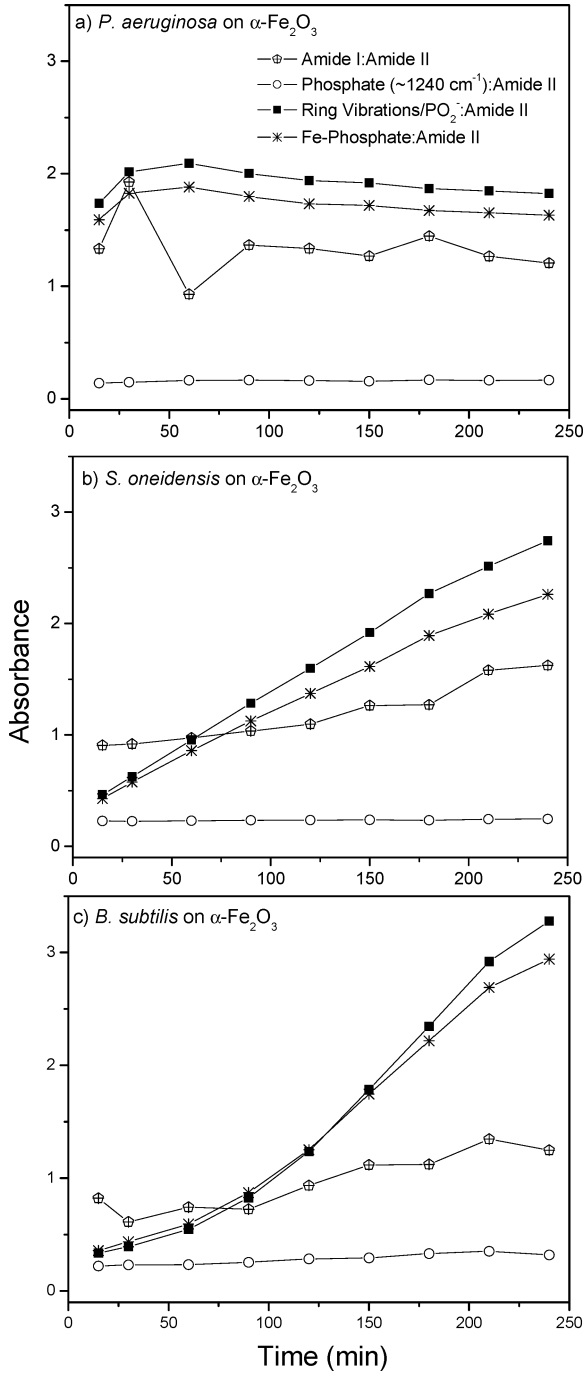

Figure 5. IR peak intensity ratios as a function of reaction time for prevalent bacterial surface functional groups of (a) *P. aeruginosa*, (b) *S. oneidensis*, and (c) *B. subtilis* on a α-Fe_2O_3-coated ZnSe surface.

< 4;[53] therefore, at pH 7, the IRE is negatively charged and adhesion of protonated amine groups would be favored. Indeed, surface proteins of *P. putida* (GB-1) have been shown to play an important role in adhesion and biofilm growth on ZnSe under flow through conditions.[44] For GB-1 cells, a large decrease in adhesion to ZnSe resulted from precipitation of biogenic Mn-oxides on the cell surface, which presumably resulted in blocking of protein functional groups. Although electrostatics are not solely responsible for cell adhesion, bonding interactions (e.g., protein binding, hydrogen bonding, hydrophobic interaction) must overcome the repulsion between like-charged bacteria and surfaces in order for adhesion to occur.[5,13,15,74]

4.2. Sorption-Induced Protonation of Carboxylate. Carboxylic groups are predominantly dissociated at pH 7 (pK_a < 5).[75] Therefore, the presence of a peak at ~1720 cm^{-1} corresponding to ν_{as}(COOH) is surprising initially, given the circumneutral conditions of the study (pH ~ 7; Figure 3b). Nonetheless, distinct peaks (~1720 cm^{-1}) were observed for *S. oneidensis* and *P. aeruginosa* aggregated with colloidal α-Fe_2O_3. This result was reproducible in triplicate experiments, despite variable ν_{as}(COOH) peak intensity. In the case of *B. subtilis*, a peak at 1720 cm^{-1} appeared once, but the intensity was low relative to background. The point of zero net proton charge of α-Fe_2O_3 is between 8.0 and 8.5 and, therefore, it is positively charged at pH 7.[10] The emergence of a peak at 1720 cm^{-1}, therefore, suggests H-bridging from the mineral surface to bacterial COO^-. This may occur via direct bonding of carboxylate to surface OH groups or through water bridging. Since carboxylic groups are dissociated at pH 7, conditions are favorable for their interaction with sorbed protons associated with mineral surface hydroxyls. Hence, we conclude that the emergence of the peak at 1720 cm^{-1} is diagnostic of proton complexation at carboxylate groups of sorbed biomolecules, and that this reaction may contribute to the overall energetics of cell adhesion. Comparable results have been reported previously. For example, Duckworth and Martin[76] observed a peak at 1720 cm^{-1} for oxalate (pH 5.0) bound to α-Fe_2O_3.

4.3. Fe−Phosphate Complexation. In all spectra where α-Fe_2O_3 was present, the appearance of Fe-complexed phosphate groups (~1016 and 1041 cm^{-1}) and increased contributions from ring structures/phosphate (~1085 cm^{-1}) implicate their involvement in binding to α-Fe_2O_3 films and/or colloidal particles (Figure 4, Figure 5, Table 2). Spectra of cell-mineral colloid aggregates (Figure 4b) show bands at ~1016 cm^{-1}. Methylphosphonic acid interaction with goethite particles also produced a ν(P−OFe) peak at this frequency (1015 cm^{-1}), which was attributed to bridging-bidentate complex formation.[70] The peak at ~1016 cm^{-1} cannot be assigned unambiguously to P−OFe; it may also represent ring vibrations of DNA sugars.[62] However, since the peak is absent for bacteria on ZnSe, we interpret it as signaling P−OFe bonding. We also observed similar modes in spectra of EPS bonded to Fe-oxides,[25] and noted high preferential sorption of P-containing moieties in batch uptake studies.[33] For Gram-positive *B. subtilis* aggregated with α-Fe_2O_3, the increased spectral contribution of this peak (confirmed with triplicate experiments) relative to Gram-negative cells likely results from the additional contribution of Fe binding by teichoic acids. These molecules, which occupy a significant fraction of the cell external surface in Gram-positive bacteria, comprise terminal phosphate groups attached to glycerol and a C side chain.[77] In prior studies of Fe adsorption to *B. subtilis* cell walls, a high capacity of aqueous Fe removal was observed and attributed to sorption via phosphodiester, carboxylic, phosphoric, and hydroxyl sites.[78,79]

Interaction of bacteria with α-Fe_2O_3 films resulted in very similar spectra for all three bacteria with each showing strong ν(P−OFe) modes (1041 cm^{-1}). Kinetic data demonstrate time-dependent bacterial phosphate binding to the α-Fe_2O_3 films, particularly for *S. oneidensis* (Figure 5b) and *B. subtilus* (Figure

(74) Appenzeller, B. M. R.; Duval, Y. B.; Thomas, F.; Block, J. C. *Environ. Sci. Technol.* **2002**, *36*, 646.
(75) Martell, A. E.; Smith, R. M. *Critical Stability Constants*; Plenum Press: New York, 1977.
(76) Duckworth, O. W.; Martin, S. T. *Geochim. Cosmochim. Acta* **2001**, *65*, 4289.
(77) Tallaro, K. P.; Talaro, A. *Foundations in Microbiology*; McGraw-Hill: New York, 1999.
(78) Fein, J. B.; Daughney, C. J.; Yee, N.; Davis, T. A. *Geochim. Cosmochim. Acta* **1997**, *61*, 3319.
(79) Wightman, P. G.; Fein, J. B. *Chem. Geol.* **2005**, *216*, 177.

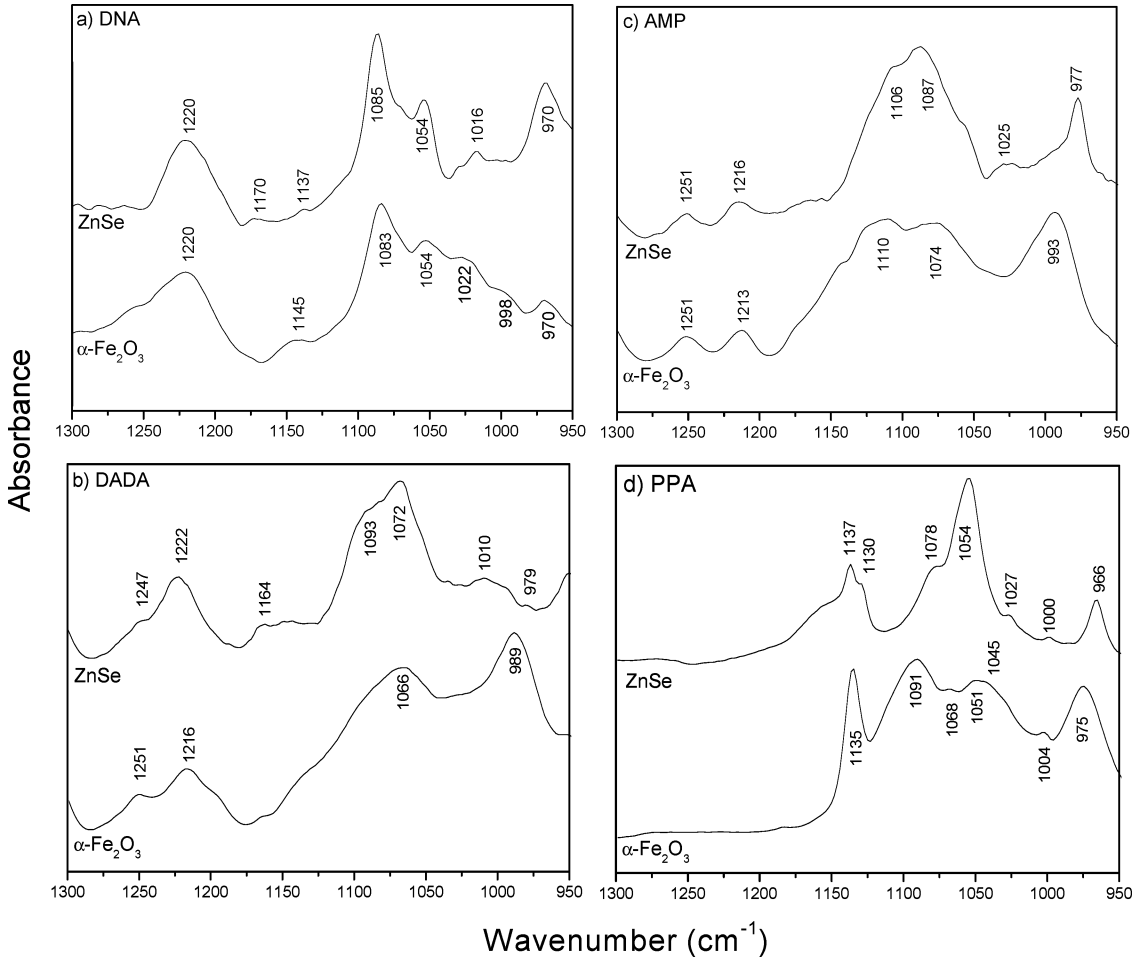

Figure 6. ATR−FTIR spectra (1300−950 cm^{-1}) of (a) DNA, (b) DADA, (c) AMP, and (d) PPA on ZnSe and α-Fe_2O_3 (all spectra collected after 120 min).

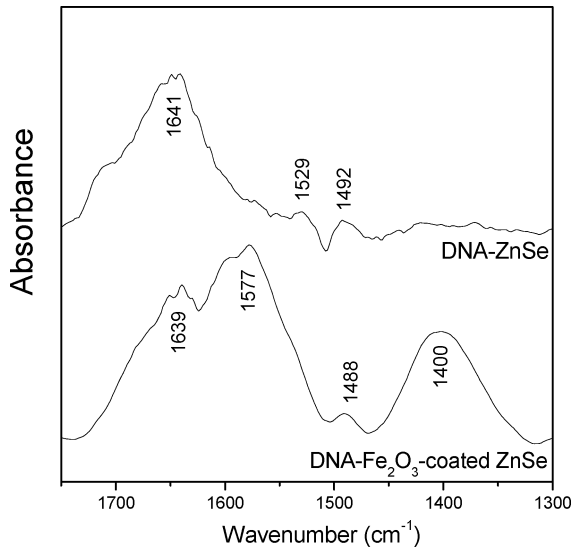

Figure 7. ATR−FTIR spectra (1750−1300 cm^{-1}) of DNA on ZnSe and α-Fe_2O_3 (all spectra collected after 120 min).

5c). Intensities of the amide I and phosphoryl, relative to the amide II, remain constant for the duration of the experiment (240 min) whereas increased intensity of Fe-phosphate and saccharide ring vibrations, relative to the amide II, are observed with increased reaction time. The similar peak intensity ratios and time-dependent trends support the notion that these peaks arise from a single group of molecules comprised of both saccharide ring structures and phosphate groups, the most likely candidate being phosphodiester groups of nucleic acids.[80] Peaks in this region (∼1030−1045 cm^{-1}) have been attributed to innersphere monodentate (and possibly bidentate bridging) complexes arising from glycophosphate and aminomethylphosphonic acid adsorption to goethite.[69,81] The growth of IR bands (1085 and 1037 cm^{-1}) corresponding to monodentate, innersphere complexation of phosphodiester groups was corroborated via quantum chemical calculations performed in conjunction with experimental studies of *B. subtilis* and *P. aeruginiosa* EPS adhesion to goethite.[25] The results presented here show that whole cell adhesion to α-Fe_2O_3 occurs via an analogous innersphere, phosphate group ligand-exchange mechanism.

It is important to note that our experiments were conducted under oxic conditions and that anoxic conditions may induce different modes of bonding for live cells. For example, adhesion of *S. oneidensis* to goethite under anoxic conditions (favorable for dissimilatory Fe reduction) leads to an increased adhesion force, and other mechanisms (e.g., specific protein adsorption) may play a significant role under such conditions.[82]

4.4. Interaction of DNA and Model P-Containing Compounds with α-Fe_2O_3. Bacterial cell samples are chemically heterogeneous, and as a result, weak IR modes may be masked by others giving rise to more intense vibrations at similar frequency. This likely contributes to the spectral structure of the mixed phosphate/polysaccharide region (1200−900 cm^{-1}), where

(80) Stryer, L. *J. Mol. Biol.* **1965**, *13*, 482.
(81) Barja, B. C.; Afonso, M. D. *Environ. Sci. Technol.* **2005**, *39*, 585.
(82) Lower, S. K.; Hochella, M. F.; Beveridge, T. J. *Science* **2001**, *292*, 1360.

several overlapping bands occur. From the data presented here and in Omoike et al.,[25] it is apparent that interactions of bacterial cells or their extracellular polymers with Fe-oxide surfaces are unique relative to both ZnSe and Ge materials, which constitute the IREs used in this study and in Omoike et al.,[25] respectively. Phosphate groups clearly play an important role in this difference.

DNA, DADA, AMP, and PPA were used as models for surficial and extracellular P-containing biomolecules that could contribute to the observed differences in IR spectra. DNA and DADA both contain phosphodiester bonds, AMP has a terminal phosphate group, and PPA has a terminal phosphonic group (Figure 1). The terminal phosphate group (PO_4^{2-}) of AMP differs from that of the phosphonic group (PO_3^{2-}) in PPA in that, for the former, the phosphorus is attached to the carbon ring via a phosphodiester bond, giving it greater rotational freedom (Figure 1). Though such differences are also reflected in IR spectra, we do not know the extent to which they translate to different reactivity toward Fe oxide surfaces. In any case, examination of IR spectra resulting from reaction of these model compounds with α-Fe_2O_3 surfaces under conditions similar to those used for the cell-mineral studies facilitates confirmation of peak assignments and bonding mechanisms.

DNA is a common component of EPS[18] and could potentially play a valuable role in conditioning film formation and cell adhesion to Fe-oxide surfaces.[25] Extracellular DNA may result from cell lysis[32] or exudation.[28,83] DNA molecules are comprised of two strands of phosphodiester-containing nucleotides linked via H-bonding to form a double helix configuration. Purine and pyrimidine bases are within the double helix while phosphate and deoxyribose units reside on the periphery.[84] In this conformation, DNA bases are not available for direct interaction with surfaces. However, ATR-FTIR spectra in Figure 7 clearly show a change in the amide (base) region (1500−1700 cm^{-1}) upon DNA reaction with α-Fe_2O_3. Similar changes in DNA base vibrations were reported for calf-thymus DNA reacted with aqueous Fe(III).[85] This effect was attributed to Fe(III)-induced auto-oxidation of DNA and the subsequent availability of bases for reaction with Fe(III). Oxidative cleavage of DNA via Fe(III) is also documented elsewhere.[86−88] The spectrum of DNA on α-Fe_2O_3 contains a large peak at 1400 cm^{-1} [$\upsilon_s(COO^-)$]. This peak provides further evidence for DNA oxidation in that it likely derives from ribose ring cleavage. The presence of anionic carboxylate groups on oxidized DNA could contribute to subsequent bonding at positive-charged Fe oxide surfaces.

The IR data for model P compounds also shed some light on the results of Omoike et al.[25] When EPS from *B. subtilis* and *P. aeruginosa* was reacted with goethite, new IR peaks emerged at 1137, 1037, and 997 cm^{-1}. These peaks were accompanied by growth in the peak at 1085 cm^{-1}. As noted above, the peaks at ∼1085 and ∼1037 cm^{-1} are observed in the present study upon introduction of whole bacterial cells to α-Fe_2O_3. The peak at ca. 1137 cm^{-1}, corresponding to ν(P═O), is also observed in the spectra of DNA and PPA (Figure 6). Interaction of DNA with α-Fe_2O_3 results in a new peak at 1141 cm^{-1} (Figure 6a). In the case of PPA, the peak is present in both ZnSe and α-Fe_2O_3 spectra. However, upon reaction with α-Fe_2O_3 there is a slight shift (to 1135 cm^{-1}) and an increase in relative peak intensity. This likely signals the bonding of phosphonate to the α-Fe_2O_3 surface. The peak located at 1045 cm^{-1} for PPA-Fe_2O_3 is assigned to monodentate P−OFe bonding based on previous molecular modeling results.[25] This peak arises close to that observed in bacteria-Fe_2O_3 systems (1041 cm^{-1}; Figure 4c). Strong binding of phosphonate with Fe(III) has been demonstrated previously.[70,89]

The peak at 997 cm^{-1}, also observed for EPS interaction with FeOOH,[25] is present in IR spectra of DNA (998 cm^{-1}), DADA (989 cm^{-1}), and AMP (993 cm^{-1}) sorbed to α-Fe_2O_3 (Figure 6). The peak is absent for spectra of these same compounds on ZnSe. These results strongly suggest a unique role for Fe in the bonding of phosphate-containing EPS and cell surface moieties at mineral surfaces. The electron density of P−OFe exceeds that of P−OH and hence gives rise to higher vibrational frequencies.[70] As a result, a shift to higher wavenumber is observed for peaks located between 970 and 1000 cm^{-1} upon formation of metal complexes. In the case of AMP (Figure 6c), the P−OH peak (977 cm^{-1} on ZnSe) is shifted to 993 cm^{-1} (P−OFe). Spectra for bacteria and P-containing compounds on α-Fe_2O_3 films give absorbances corresponding to the four major peaks observed during EPS adsorption to α-FeOOH.[25] In all cases, the most likely explanation for the observed results is monodentate, inner-sphere complexation of phosphoryl groups at Fe metal centers.

5. Conclusions

ATR-FTIR experiments reveal significant short-range bonding interactions occur upon adhesion of both Gram negative and Gram positive bacterial cells to the positive-charged hematite surface. Although nucleic acids and/or surface proteins appear to mediate bacterial adhesion to ZnSe surfaces, attachment to α-Fe_2O_3 films involves a change in protein conformation/composition and the formation of innersphere P−OFe bonds. Aggregation of bacterial cells in colloidal suspension with α-Fe_2O_3 also gives rise to P−OFe bond formation. Thus, in addition to attractive long-range electrostatics, coordinative Fe bonding of phosphate groups present in cell surface molecules contributes to the strong adhesion and diminished mobility that is observed when bacterial cells are introduced into Fe oxide-bearing media.

Acknowledgment. We thank Philip L. Anderson of the University of Arizona Materials Labs for performing XRD scans. We are also grateful to David Bentley of the University of Arizona Biotechnology Imaging Facility for assistance with TEM imaging and two anonymous reviewers whose constructive critiques led to significant improvement of the manuscript. This research was supported by the National Science Foundation CRAEMS program (Grant CHE-0089156).

LA061359P

(83) Brown, M. R. W.; Foster, J. H. S.; Clamp, J. R. *Biochem. J.* **1969**, *112*, 521.

(84) Stryer, L. *Biochemistry*; W. H. Freeman and Company: New York, 1995; p 1064.

(85) Ouameur, A. A.; Arakawa, H.; Ahmad, R.; Naoui, M.; Tajmir-Riahi, H. A. *DNA Cell Biol.* **2005**, *24*, 394.

(86) Adachi, S.; Yoshida, S.; Kawamura, K.; Takahashi, M.; Uchida, H.; Odagiri, Y.; Takemoto, K. *Carcinogenesis* **1994**, *15*, 753.

(87) Neves, A.; Terenzi, H.; Horner, R.; Horn, A.; Szpoganicz, B.; Sugai, J. *Inorg. Chem. Commun.* **2001**, *4*, 388.

(88) Hemmert, C.; Pitie, M.; Renz, M.; Gornitzka, H.; Soulet, S.; Meunier, B. *J. Biol. Inorg. Chem.* **2001**, *6*, 14.

(89) Barja, B. C.; Herszage, J.; Alfonso, M. D. *Polyhedron* **2001**, *20*, 1821.